SANDIA REPORT

SAND2015-8531
Unlimited Release
Printed October 2015

Ion-Conduction Mechanisms in NaSICON-Type Membranes for Energy Storage and Utilization

Anthony H. McDaniel, Jon F. Ihlefeld, Norman C. Bartelt

Prepared by
Sandia National Laboratories
Albuquerque, New Mexico 87185 and Livermore, California 94550

Sandia National Laboratories is a multi-program laboratory managed and operated by Sandia Corporation, a wholly owned subsidiary of Lockheed Martin Corporation, for the U.S. Department of Energy's National Nuclear Security Administration under contract DE-AC04-94AL85000.

Issued by Sandia National Laboratories, operated for the United States Department of Energy by Sandia Corporation.

Available to DOE and DOE contractors from
U.S. Department of Energy
Office of Scientific and Technical Information
P.O. Box 62
Oak Ridge, TN 37831

Telephone: (865) 576-8401
Facsimile: (865) 576-5728
E-Mail: reports@osti.gov
Online ordering: http://www.osti.gov/scitech

Available to the public from
U.S. Department of Commerce
National Technical Information Service
5301 Shawnee Rd
Alexandria, VA 22312

Telephone: (800) 553-6847
Facsimile: (703) 605-6900
E-Mail: orders@ntis.gov
Online order: http://www.ntis.gov/search

SAND2015-8531
Unlimited Release
Printed October 2015

Ion-Conduction Mechanisms in NaSICON-Type Membranes for Energy Storage and Utilization

Anthony H. McDaniel
Hydrogen & Combustion Technology Department
Sandia National Laboratories
P.O. Box 969
Livermore, California 94550-MS9052

Jon F. Ihlefeld
Electronic, Optical, & Nano Materials Department
Sandia National Laboratories
P.O. Box 5800
Albuquerque, New Mexico 87185-MS1069

Norman C. Bartelt
Materials Physics Department
Sandia National Laboratories
P.O. Box 969
Livermore, California 94550-MS9161

Abstract

Next generation metal-ion conducting membranes are key to developing energy storage and utilization technologies like batteries and fuel cells. Sodium super-ionic conductors (aka NaSICON) are a class of compounds with $AM_1M_2(PO_4)_3$ stoichiometry where the choice of "A" and "M" cation varies widely. This report, which describes substitutional derivatives of NZP ($NaZr_2P_3O_{12}$), summarizes the accomplishments of a Laboratory Directed Research and Development (LDRD) project to analyze transport mechanisms using a combination of *in situ* studies of structure, composition, and bonding, combined with first principles theory and modeling. We developed an experimental platform and applied methods, such as synchrotron-based X-ray spectroscopies, to probe the electronic structure of compositionally well-controlled NaSICON films while in operation (*i.e.*, conducting Na ions exposed to oxygen or water vapor atmospheres). First principles theory and modeling were used to interpret the experimental observations and develop an enhanced understanding of atomistic processes that give rise to, and affect, ion conduction.

ACKNOWLEDGMENTS

The authors gratefully acknowledge Farid El Gabaly, Josh Sugar, and Josh Whaley at Sandia Labs Livermore and Mia Blea-Kirby, William Meier, Emily Gurniak, and Bonnie B. McKenzie at Sandia Labs Albuquerque for their contribution to this project. The authors acknowledge Hendrik Bluhm, Tolek Tyliszczak, and Andrey Shavorskiy from Lawrence Berkeley National Laboratory for their assistance with experiments at the Advance Light Source. The authors also acknowledge Tsu-Chien Weng from the Stanford Synchrotron Radiation Lightsource for his assistance with experiments at SSRL.

CONTENTS

FIGURES

NOMENCLATURE

ALS	Advanced Light Source
APPES1	ambient pressure photo-electron spectroscopy chamber at ALS
CSD	chemical solution deposition
DFT	Density Functional Theory
EIS	electrical impedance spectra
FY	fluorescence yield
HREELS	high resolution electron energy loss spectroscopy
ICSD	Inorganic Crystal Structure Database
LBNL	Lawrence Berkeley National Laboratory
NaSICON	sodium superionic conductor
NZP_Al	$Na_{1+x}Al_xZr_{2-x}P_3O_{12}$
NZP	$NaZr_2P_3O_{12}$
NZP_Si	$Na_{1+x}Zr_2Si_xP_{3-x}O_{12}$
PEY	partial electron yield
SNL	Sandia National Laboratories
SSRL	Stanford Synchrotron Radiation Lightsource
TEM	transition electron microscopy
VASP	Vienna Ab initio Simulation Package
XAS	X-ray absorption spectra

1. INTRODUCTION

Next generation metal-ion conducting membranes are critical components of the metal-air batteries and flow batteries that will enable grid-scale electrical energy storage. Such technologies are important to fully integrating intermittent renewable energy sources into the U.S. infrastructure. NaSICON-type materials having the stoichiometry $NaZr_2P_3O_{12}$ (NZP), $Na_{1+x}Zr_2Si_xP_{3-x}O_{12}$ (NZP_Si), and $Na_{1+x}Al_xZr_{2-x}P_3O_{12}$ (NZP_Al) are of particular interest because they can be used as both a solid electrolyte and electrode in sodium-based air-breathing batteries. A vast array of other NaSICON stoichiometries are possible by exchanging the cations with alkali, alkaline earth, p-group, and transition metal ions.(1) Other than stoichiometry, the defining feature of NaSICON is the formation of a 3-D crystallographic framework that contains interconnected channels within which mobile cations are conducted. It is supposed that crystallographically-defined bottlenecks within the network limit transport, and that the NaSICON stoichiometry ultimately governs sodium diffusion rates.(2) The challenge is to design NaSICON with optimal ion mobility and chemical stability. Current research is mired in a heuristic approach to probing the enormous array of possible material compositions that manifest ion conductivity in NaSICON. A comprehensive atomic-level picture of the factors that influence ion conduction is missing.

The objective of this LDRD is to analyze transport chemistry using a combination of *in situ* studies of structure, composition, and bonding, combined with first principles theory and modeling, to develop an atomistic understanding of mechanisms that give rise to and/or influence sodium ion conductivity. Specifically, we seek answers to the following questions:

What are the pathways and energy barriers for Na^+ transport in NaSICON?

How does the addition of Si into $Na_{1+x}Zr_2Si_xP_{3-x}O_{12}$, and Al into $Na_{1+x}Al_xZr_{2-x}P_3O_{12}$, affect electronic structure and Na^+ conductivity?

Does exposure to water vapor lead to NaSICON protonation and affect Na^+ transport?

In this report, we document an integrated experimental and theoretical effort to decipher the atomistic processes that govern ion conduction. Transport chemistry is analyzed using X-ray diagnostics on well-controlled, model material systems fabricated through thin film growth methods. First principles theory and modeling are used to interpret these experiments thus providing the necessary link between electronic structure and ionic transport.

2. ACCOMPLISHMENTS

The objective of this project was to analyze transport chemistry in solid-state sodium super ionic conductors using a combination of *in situ* studies of structure, composition, and bonding, combined with first principles theory and modeling. In order to accomplish these objectives, we first developed a chemical solution deposition (CSD) process to synthesize hundreds of nm-thick films of NZP, NZP_Si, and NZP_Al with well controlled stoichiometry and of known purity and crystallinity. We then built an environmental chamber for conducting electrochemical experiments in conjunction with X-ray Raman spectroscopy, and deployed this apparatus at beamline 6-2, Stanford Synchrotron Radiation Lightsource (SSRL). We also constructed a thermally-robust fluorescence yield (FY) detector for measuring X-ray absorption spectra and deployed it at beamline 11.0.2, Advanced Light Source (ALS), Berkeley, CA. The electrochemical behavior of NaSICON films at elevated temperature and in low pressure O_2 or H_2O environments was studied using hard and soft X-ray spectroscopies at each synchrotron, respectively.

Finally, the VASP DFT code was used to resolve the energy landscape of sodium in specific NaSICON formulations. Initial work focused on locating the sodium ion's low energy binding sites within the lattice. This information was used to interpret the X-ray absorption spectroscopies by providing electronic structure models inputted to an *ab initio* multiple scattering code (FEFF90).(3) Calculated spectra were then compared to experiment, essentially validating the DFT-based models. The effects of substitution on electronic structure and diffusion barriers for sodium motion were then explored with the intent of understanding how to improve conductivity.

2.1. Chemical Solution Deposition of NaSICON Thin Films

The solution chemistry used to prepare NaSICON thin films was based upon sol-gel chemistries reported by Gasmi *et al*.(4) and Martucci *et al*.(5) Briefly, elemental precursors in the form of alkoxides and organophosphates were dissolved in complex mixtures of alcohols and other organics to form viscous solutions that were spin cast onto platinized-Si or AlN substrates (see Figure 1). After solvent evaporation and gel consolidation, coated substrates were inserted into a preheated tube furnace (temperatures 725-800 °C) for 10 minutes in air prior to depositing subsequent layers following the same spin casting, pyrolysis, and high-temperature annealing steps. Films that were three total layers in thickness (~250 nm) were used in this work. See Meier *et al*.(6) for information regarding our CSD methodology and information describing full characterization of resultant film properties.

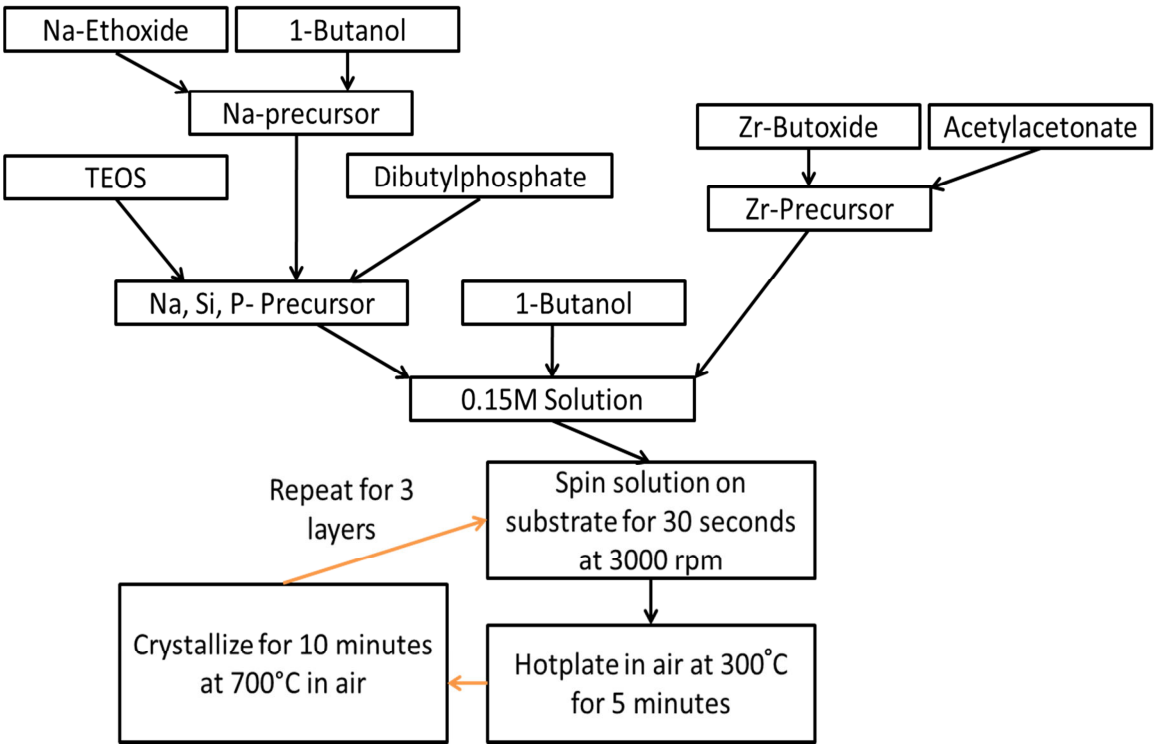

Figure 1. Flow chart showing mixing of elemental precursors, spin casting, pyrolysis, and annealing steps used to produce NaSICON thin films.

Depending on the desired NaSICON stoichiometry and annealing temperature, various film textures, ion conductivities, and phase impurities were obtained. Figure 2 summarizes these observations for representative films and processing conditions. Panels (a-c) in Figure 2 illustrate how annealing temperature changes film texture. It is clear the crystallite size increases at higher annealing temperatures. In addition, panel (e) shows that the secondary phase impurities and preferred orientation are dependent on film stoichiometry (NZP_Al in this instance though similar trends were observed in the NZP_Si variants). Finally panels (f-g) show the results of impedance measurements used to derive film conductance and measure energy barriers for sodium transport. The electrical impedance spectra (EIS) in Figure 2(f) are characteristic of a blocking-electrode response, where Na^+ ion mobility is probed by applying a 50 mVAC signal across the film at frequencies ranging from 1 MHz to 5.7 Hz. The Na^+ ions never enter or leave the solid, but by analyzing the AC current response over all frequencies, the area specific conductance can be extracted. We should note that EIS were measured *in situ* and simultaneous to the X-ray spectra during the course of our synchrotron campaigns. The data in Figure 2f-g show how composition impacts conductance; replacing a small fraction of Zr with Al causes a significant increase in Na^+ conductance. Results for NZP are detailed in Meier *et al.*(6) and those for NZP_Si in a pending submission to the Journal of the American Ceramics Society. The ability to prepare NaSICON thin films with known and well-characterized properties was a key first accomplishment in this LDRD.

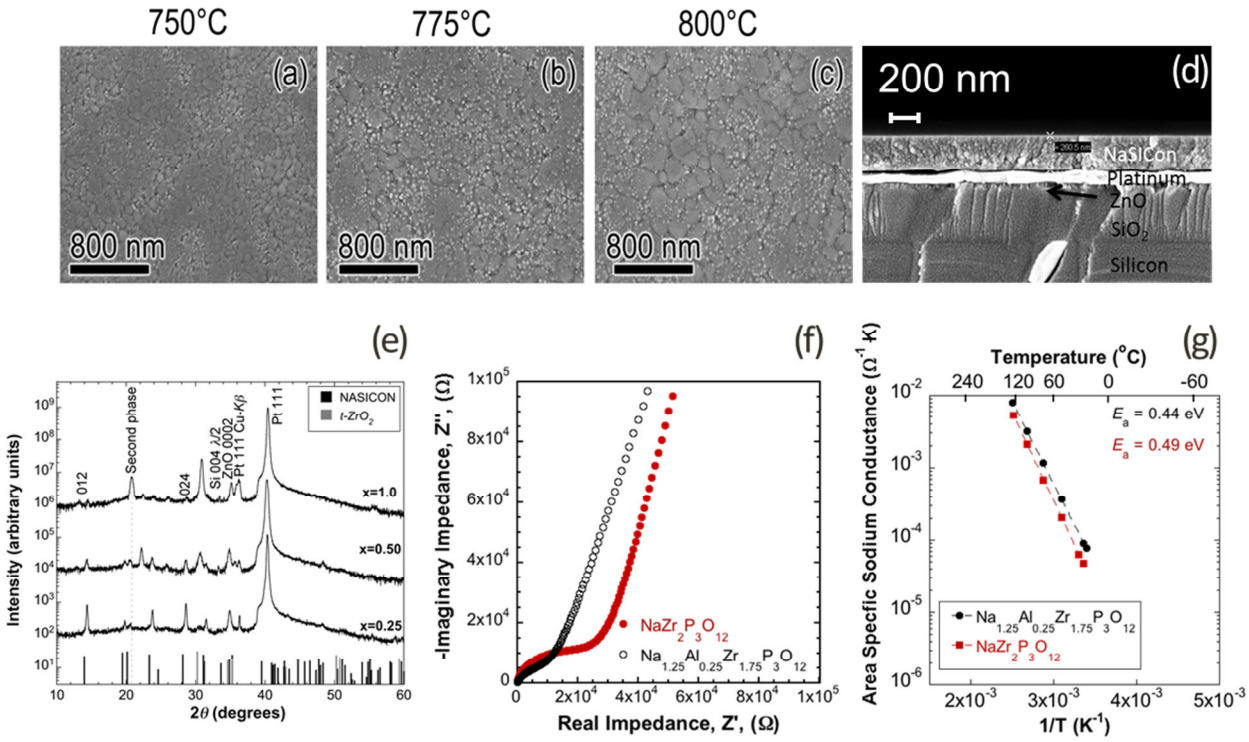

Figure 2. (a-c) SEM images of representative NaSICON films showing the effect of increasing annealing temperature on crystallite size and film texture. (d) SEM cross section of NaSICON film on platinized Si wafer showing stack complexity (NaSICON/Pt/ZnO/SiO_2/Si). Pt is used as a diffusion barrier and back side electrical contact for impedance measurements. Films were also successfully deposited on AlN substrates. (e) X-ray diffraction patterns of $NaAl_xZr_{2-x}P_3O_{12}$ as a function of Al content showing the effect of composition on texturing. Notice that the <012> orientation becomes less pronounced at higher Al fraction. (f) Representative impedance spectra for NZP and NZP_Al films measured at room temperature. (g) Area specific conductance for NZP and NZP_Al films as a function of temperature showing that substituting Al for Zr increases conductance and lowers the energy barrier (E_a) associated with Na^+ transport.

2.2. Hardware Development for X-ray Measurements

In order to examine ion transport in NaSICON using X-ray diagnostics, we had to develop and deploy an environmental chamber at one synchrotron, and construct a thermally robust photon detector for another. This enabled X-ray measurements to be conducted *in situ* with the NaSICON exposed to low pressures of either O_2 or H_2O (0.5-2.0 Torr), at above ambient temperature (>100°C), while collecting EIS simultaneous to X-ray spectroscopies.

2.2.1 Environmental Chamber Deployed at SSRL

The X-Ray absorption coefficient is particularly sensitive to coordination chemistry and elemental oxidation state.(7) It is believed that sodium colocation to oxygen during transport perturbs electron density near the lattice oxygen sites. Our approach is predicated on assessing perturbations of the local bonding environment to both the Na and O atoms in the lattice caused

by ionic conduction, chemical composition, and other environmental factors. To accomplish this, characteristic X-ray absorption spectra (XAS) for a baseline NZP composition was compared to Al- and Si-substituted variants. In addition to probing the effects of compositional variation on ion transport, we thought it important to expose the NaSICON films to thermochemical conditions typically found at the cathode side of a sodium-air battery, such as elevated temperature and oxygen or water vapor at the gas-sold interface.

One complication with using X-ray spectroscopy is that O_2 and H_2O molecules contain an O atom, which will absorb the incident X-ray photon at the O-K edge (530 eV) and produce spectral artifacts that interfere with NaSICON's O atoms. In the early part of this LDRD, we explored using an X-ray Raman technique to eliminate this interference. On SSRL's beamline 6-2, there exists a high resolution, large solid angle X-ray Raman end station.(8) Basically, tunable incident X-rays at photon energies above 6500 eV are scattered inelastically from a solid target. By measuring the energy loss between incident and detected photon for a 1s core excitation, O-K edge spectra can be recovered without interference from gas-phase species because they are transparent at the incident photon energy. Figure 3a shows a schematic of the end station, and Figure 3(b-c) show concepts for environmental chambers that would interface to the spectrometer.

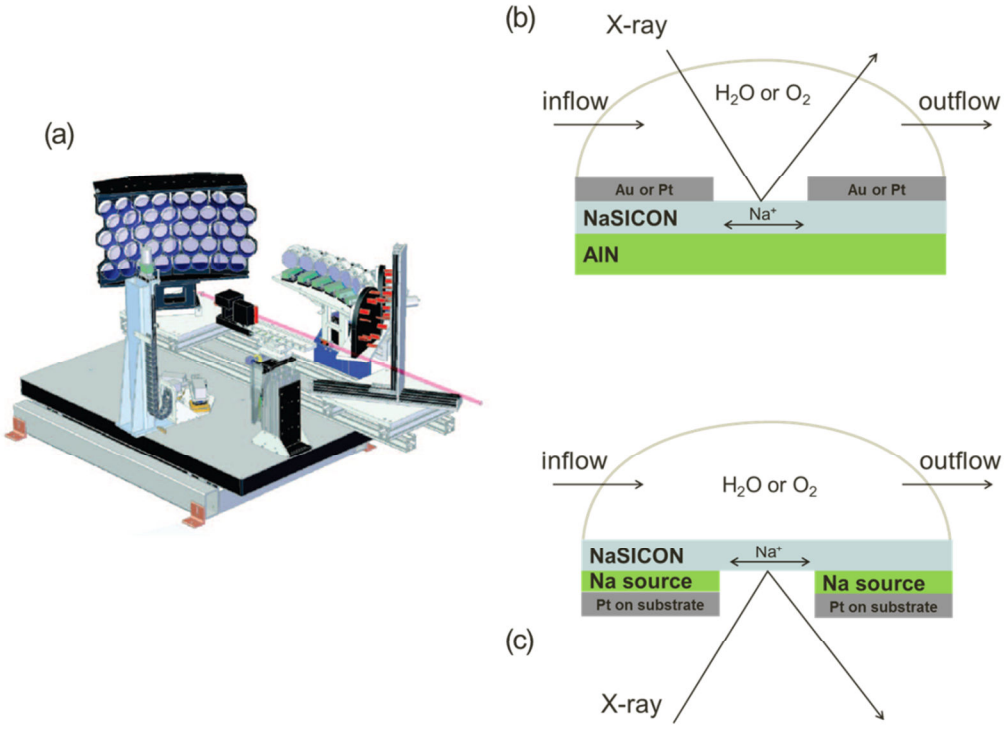

Figure 3. (a) Drawing of the X-ray Raman apparatus on beamline 6-2 at SSRL. Reprinted from reference (8) in accordance with the Creative Commons Attribution 3.0 Unported License. (b) Concept for environmental chamber designed and deployed at SSRL. Ion conduction measurements are restricted to a blocking-electrode configuration. (c) A concept for creating a second generation experimental platform for probing Na^+ conduction in a more battery-like configuration where ions can enter and exit the NaSICON under the influence of an applied field.

Ultimately we designed and deployed the apparatus depicted in Figure 4. The environmental chamber consists of a sample pedestal with integrated resistive heating element, flow lines that allow for gases to enter and exit the chamber, and electrical feedthroughs for providing power to the heater as well as contacts to the sample surface. The chamber is water cooled and covered by a PEEK plastic dome. The entirety of our experimental platform consisted of NaSICON films supported on AlN substrates and a balance of plant for regulating chamber pressure, mass flow rates of O_2 or H_2O, sample temperature, etc. (Figure 4). The environmental chamber is capable of operating at pressures between atmospheric and vacuum, and sample temperatures as high as 1000 °C.

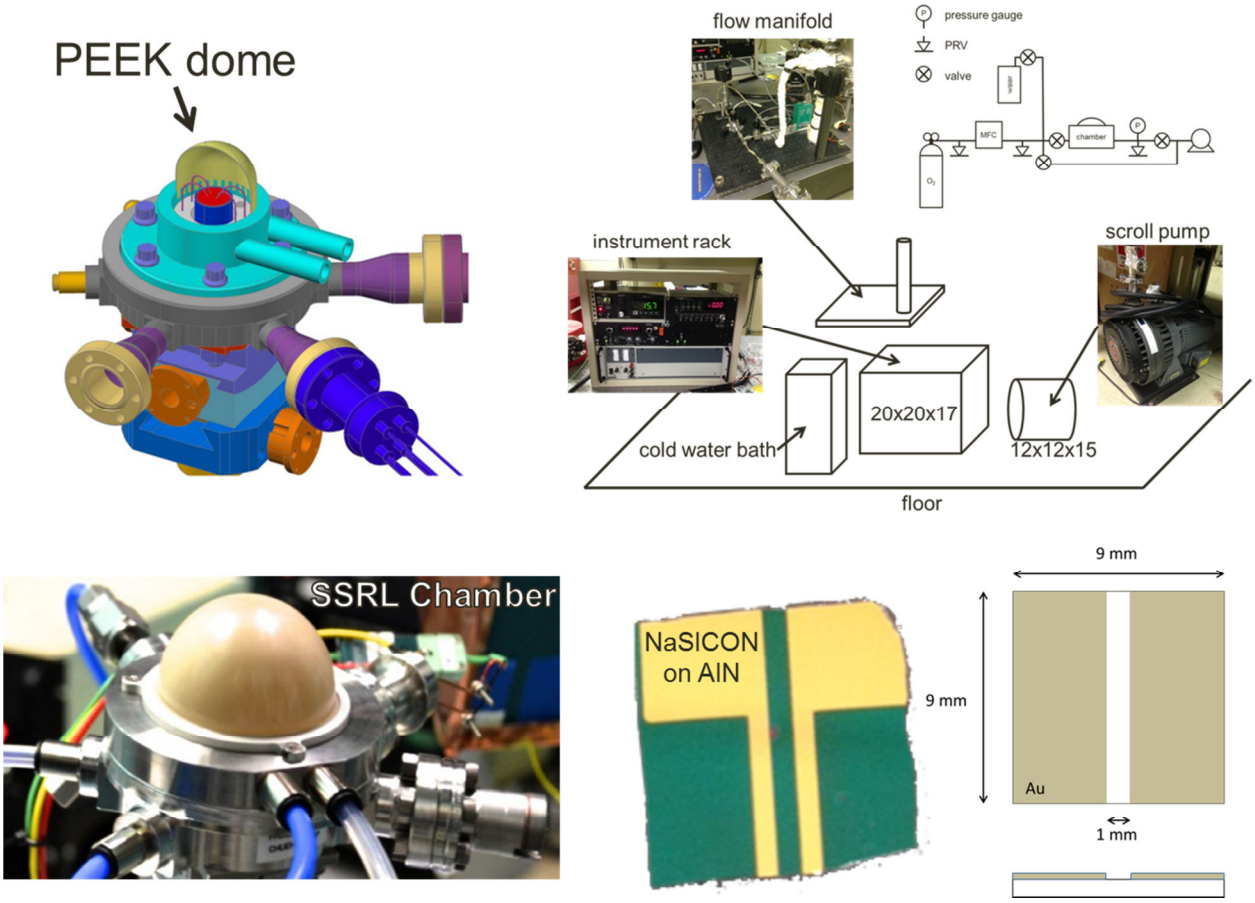

Figure 4. (lower and upper left) Photograph and solid drawing showing the custom environmental chamber designed and deployed at SSRL on beamline 6-2. The NaSICON sample mounts on a heated stage (red disc in drawing) at the center of the fixture. (lower right) NaSICON thin film supported on AlN and top coated with gold contacts. (upper right) Balance of plant for the SSRL experimental chamber with instrument rack, flow control manifold and scroll pump.

2.2.2 Robust Fluorescence Yield Detector Deployed at ALS

The aforementioned X-ray Raman measurements at SSRL met with limited success, as will be described later, therefore the majority of XAS studies were conducted on the APPES1 end

station at beamline 11.0.2, ALS, Berkeley, CA. While this world-class instrument is equipped with a bright source of soft X-rays and ambient pressure photoelectron energy analyzer, which is suitable for measuring XAS in the partial electron yield (PEY) mode, it did not house a robust fluorescence yield (FY) measurement capability. Differences between PEY and FY, namely sensitivity (based on atomic absorption cross section) and probe depth (electron vs. photon escape depth), motivated us to install the FY detector shown in Figure 5 on APPES1 in order to successfully accomplish our science objectives. The design was borrowed from a similar detector Sandia incorporated into a user chamber developed under an earlier LDRD.(9,10) The unique feature of this detector is high ambient light rejection and water cooling such that FY XAS can be measured from a high-temperature incandescent sample.

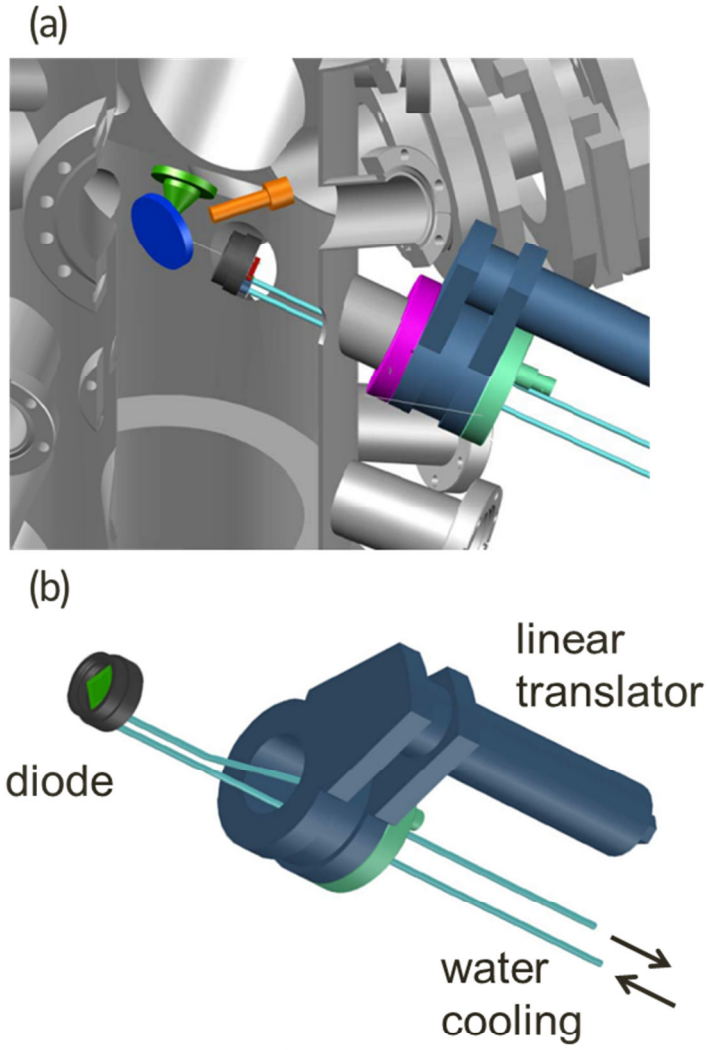

Figure 5. (a) Cut away view of APPES1 chamber on beamline 11.0.2 at ALS showing entrance cone to electron energy analyzer (green), X-ray source window (orange), sample holder (blue), and position of Sandia's FY detector. (b) Drawing of water-cooled, passive FY detector deployed at APPES1.

Adequate environmental control systems were available on APPES1, and thus we only needed to mount our NaSICON samples, as shown in Figure 6, on the APPES1 manipulator stage. While collecting XAS in the soft X-ray region (100-2000 eV) is not ideal for the O-K edge due to interference from O_2 and H_2O molecules, as mentioned in the previous section, we were able to mitigate the spectral interference by use of absorption backgrounds collected on Au foils, and operating at low gas partial pressure (100 mTorr).

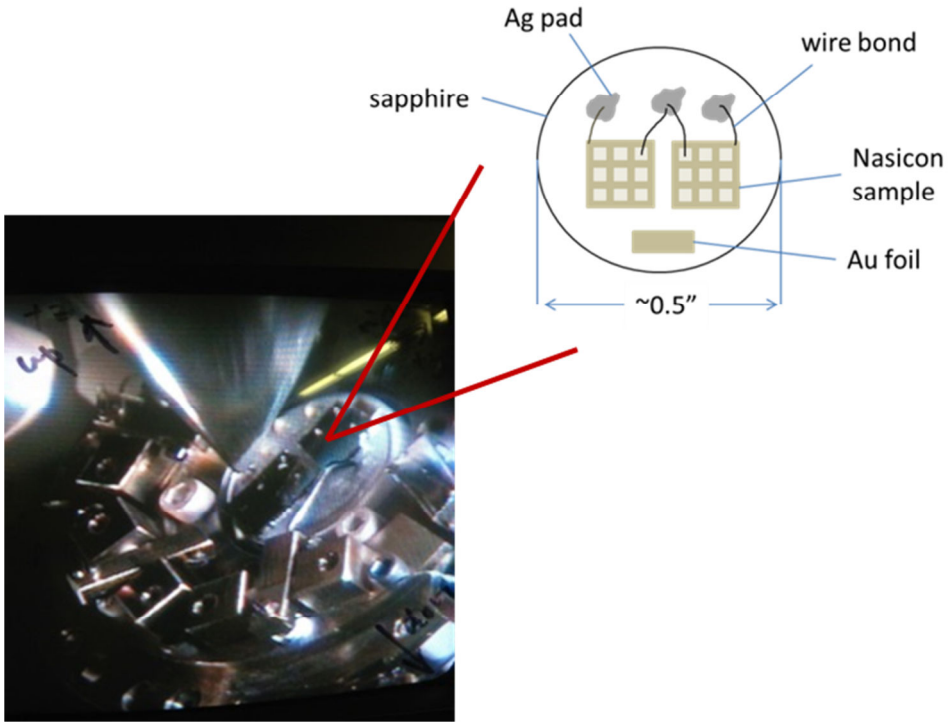

Figure 6. Picture of NaSICON sample mounted on the APPES1 manipulator stage. The sample consisted of Si-supported NaSICON films atop a sapphire disc. Wire bonds were used to contact top and bottom side of NaSICON film for EIS measurements. The Au foil was used to collect background XAS.

2.3. Results of Experimental Campaigns

During the course of this LDRD, 5 experimental campaigns were conducted at two different synchrotrons; two at SSRL and three at ALS. The hard X-ray measurements were devised to test feasibility of using X-ray Raman as an effective analytical tool. The more conventional soft X-ray spectroscopies, like X-ray absorption and ambient pressure X-ray photoelectron, were applied with greater success. Results of these campaigns, as well as scoping studies using TEM HREELS, are described next.

2.3.1 Hard X-ray Measurements at SSRL

We anticipated that the X-ray Raman technique would not only allow for measuring XAS free from gas-phase spectral interference, but also allow us to probe electronic structure of all light elements in our NaSICON system, namely O, Na, Al, Si, P. The 1s core-level electron energies

for these elements are below 2015 eV making them theoretically accessible with an excitation energy >6500 eV. And while preliminary scoping studies appeared promising on bulk commercial materials, we encountered great difficulty applying this technique to thin films and to elements with atomic numbers greater than that of O (Z=8). The results of both campaigns are summarized in Figure 7 for the O-K and Na-K absorption edges. Perhaps the most disappointing revelations were the time required to collect a single, low-noise XAS, and the poor resolution of the Na-K edge features. The spectra shown in Figure 7 took 5 hrs to collect; an O-K spectrum with sufficiently higher signal/noise ratio took longer than 15 hrs to collect (not shown). This made it practically impossible to conduct dynamic studies, or to focus on more than one element in the allotted period of time. Nonetheless, the environmental chamber is still used by collaborators at Stanford and SSRL interested in synchrotron-based surface X-ray diffraction measurements.

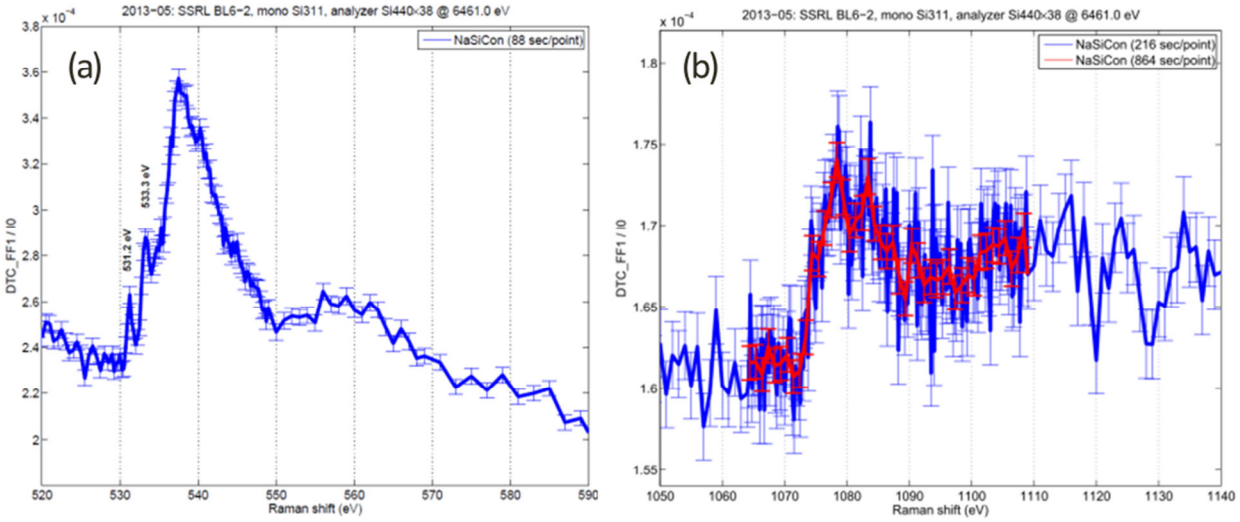

Figure 7. (a) Representative X-ray Raman spectrum for O-K edge in NaSICON after 5 hours of data collection. Ambient conditions were ~150 °C with 2 Torr O_2 pressure. (b) Spectrum of Na-K edge after 5 hours of data collection at conditions similar to (a). The signal/noise ratio is considerably worse for this technique at higher atomic number. Poor energy resolution, high noise, and low sensitivity to Z>8 limit this diagnostic approach.

2.3.2 Soft X-ray Measurements at ALS

Even with the spectral interference induced by gas overpressure from O_2 and H_2O on the O-K absorption edge, we collected considerably higher quality data in APPES1. We succeeded in measuring XAS for NZP, NZP_Al, and NZP_Si thin films exposed to 100 mTorr of either O_2 or H_2O at temperatures between 100 and 250 °C. We also collected ambient pressure photoelectron spectra in order to assess surface composition. This report will only describe the PEY and FY measurements.

Shown in Figure 8 are NZP's normalized PEY and FY XAS for the O-K edge under an ambient of either O_2 or H_2O. The raw XAS signal (I) was normalized to its respective PEY or FY beam profile (I_o) collected in vacuum or in the presence of gases from Au foil targets. Baselines were subtracted and spectra flattened using the method described by Manceau *et al.*,(11) after which

spectra were scaled to the value of the atomic mass attenuation coefficient(12) far from the absorption edge. It is worth noting that the EIS (i.e., ion conductivities) were not significantly different between the two test conditions (O_2 vs. H_2O), though the length of time our films were exposed to water vapor may not have been sufficient to perturb bulk properties, particularly under the electrode where significant lateral diffusion would be necessary.

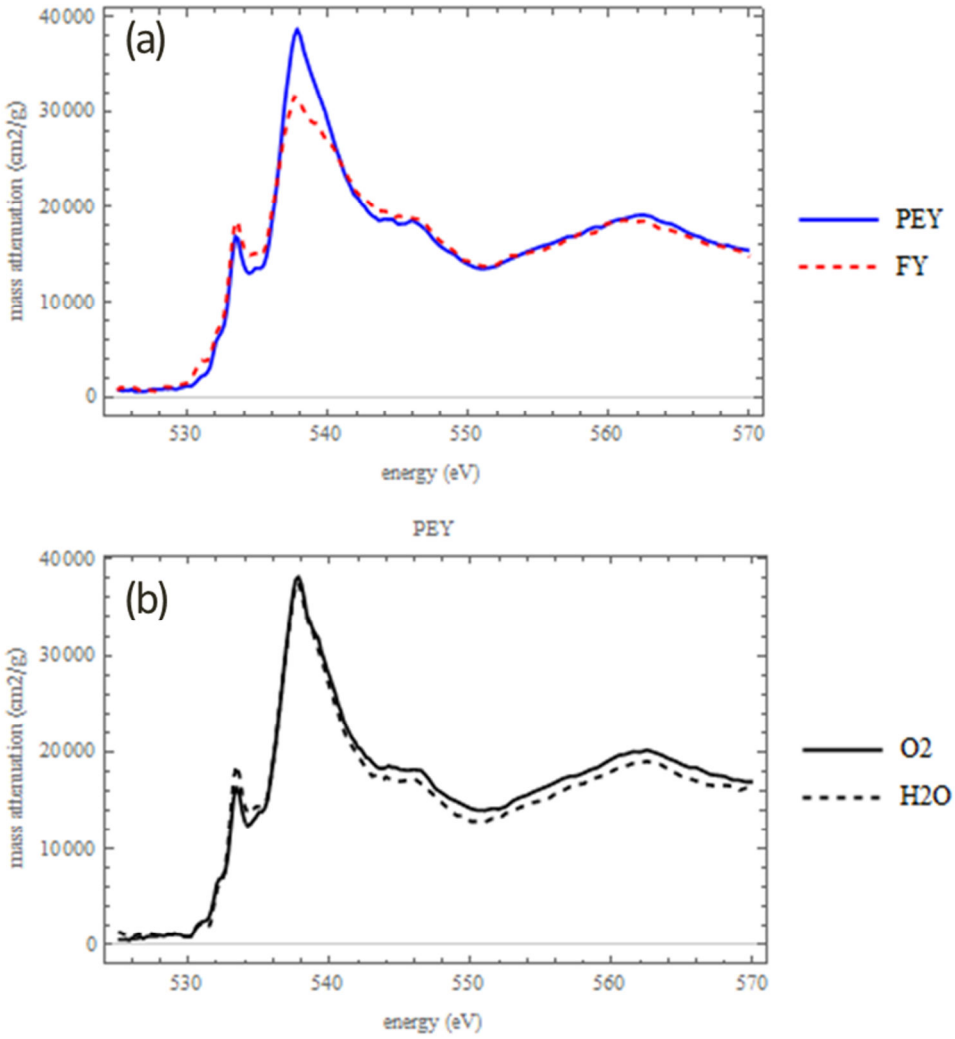

Figure 8. (a) Normalized O-K edge PEY and FY XAS for a 250 nm thick NZP film under 100 mTorr O_2 at 150°C. The difference between intensity of near edge features between PEY and FY may be due to self-absorption of the fluoresced photon. (b) Normalized PEY XAS for same film comparing O_2 and H_2O ambient conditions. In the time required to collect spectra (of order hours), there is no clear indication of a change in electronic structure due to H_2O exposure.

Consulting the XAS data in Figure 8, there is an obvious difference in the spectral intensity between PEY and FY at 538 eV. This is likely due to self-absorption in the FY measurement, and is a known issue with optically "thick" samples. Correction methods do exist, and we are looking into methods for removing this artifact. Also, there are no obvious differences between

O_2 and H_2O, which is consistent with the same null result observed in the EIS (not shown). Similar trends shown in Figure 8(a, b) were observed with NZP_Al and NZP_Si.

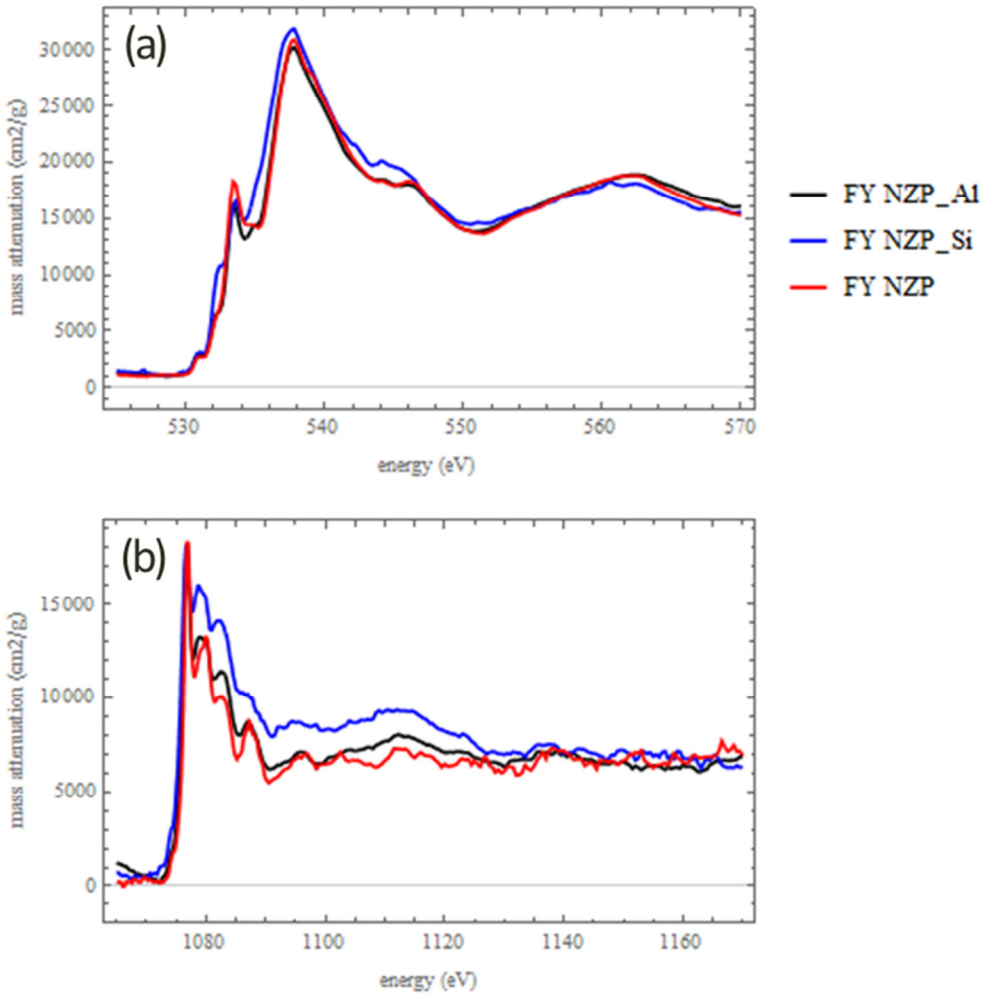

Figure 9. (a) Normalized O-K edge FY XAS for ~250 nm thick NZP, NZP_Al, and NZP_Si films under 100 mTorr O_2 at 150°C. There are clear differences in the near-edge absorption features indicating that Al and Si substitution perturb the local electronic structure of the O-atom relative to NZP. (b) Normalized Na-K edge FY XAS for same films also show that the bonding environment local to Na atoms is changed by substitution.

The effects of film composition, as shown in Figure 9, are very pronounced and indicate that fractional substitution of Al for Zr, and Si for P, change the bulk electronic properties of our NaSICON films. In both the O (Figure 9(a)) and Na (Figure 9(b)) XAS, spectral density in the near edge region (+/-20 eV nearest the edge jump) differs between NZP, NZP_Al, and NZP_Si. This region is dominated by local scattering phenomena and is most sensitive to variations in bond lengths between target atom and nearby scattering atoms, as well as the identity of the nearest-neighbor atoms. These observations will be used to validate DFT electronic structure models.

2.3.3 TEM HREELS Measurements at Sandia

While we had great success using soft X-ray diagnostics as a means to reveal atomistic relationships between chemical composition and electronic structure, we were faced with the reality that limited access to synchrotrons, ALS in particular, was problematic. As with the hard X-ray Raman diagnostic, we tested the feasibility of using TEM high-resolution electron energy loss spectroscopy (HREELS) as a means to supplement the soft X-ray information. From the perspective of the scattering processes, HREELS (electron-in, electron-out) provides identical information to XAS (photon-in, photon-out or photon-in, electron-out). The open question with TEM is the same as with X-ray Raman, *is the approach suitable to studying NaSICON?* With TEM, there is a concern about electron damage of the material under study, and the inability to conduct *in situ* experiments. Here powders were used instead of films, and the results are summarized in Figure 10.

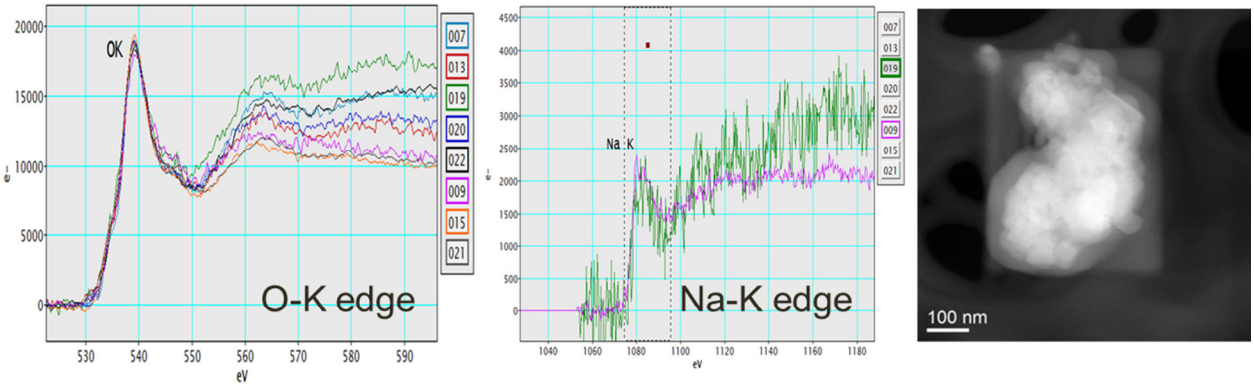

Figure 10. (left to right) Representative TEM HREELS spectra for O-K edge, Na-K edge, and a TEM image of NaSICON powder. Poor energy resolution, a propensity for beam damage, and the inability to probe materials *in situ* limit this diagnostic approach.

Unfortunately, as with X-ray Raman, the TEM HREELS approach will require more time for method development in order to be useful. Beam damage was obvious, and the electron energy resolution at both absorption edges was unsatisfactory for modeling purposes.

2.4. Application of Theory and Modeling

The X-Ray absorption coefficient is particularly sensitive to coordination chemistry and oxidation state. In order to develop a deeper understanding of the effects of Al and Si substitution into NZP, the VASP DFT(13–16) code was used to formulate electronic structure models for our NaSICON compositions and then predict the XAS using an *ab initio* multiple scattering code (FEFF90).(3) We are currently working towards validating these models against measured XAS, the results of which will be the topic of a future technical paper. Thus far, DFT modeling of Na^+ transport in this system has revealed an extreme sensitivity to lattice parameter suggesting that appropriately chosen substitutional defects could considerably increase ion conductivity.

2.4.1 Calculation of X-ray Spectra with FEFF90

FEFF90 is an *ab initio* self-consistent real space multiple scattering code we used to calculate X-ray absorption spectra. This parameter-free model includes polarization dependence, core-hole effects, and local field corrections, based on self-consistent, spherical muffin-tin scattering potentials.(3) One particular challenge we faced with the NZP_Al and NZP_Si systems is local heterogeneity induced by alloying the NZP crystal structure. The FEFF90 model calculates the XAS for a specific target atom, subject to scattering by nearest neighbor atoms. In order to accurately predict the observed XAS, we had to sample a modest number of possible scattering configurations for Na and O, and then take a weighted average of each calculated XAS to account for multiple effects in a heterogeneous environment. This methodology is briefly outlined in Figure 11.

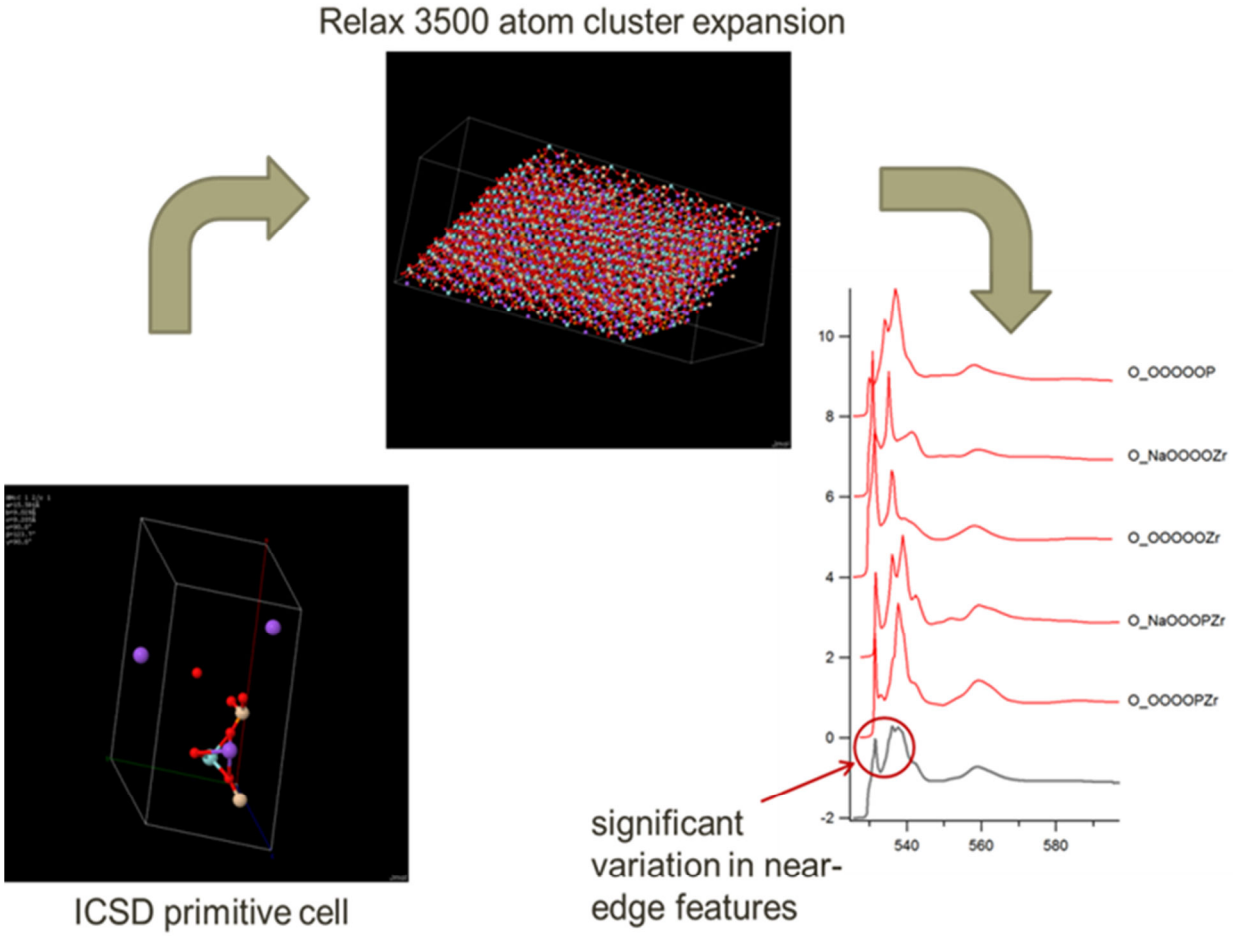

Figure 11. Diagram illustrating the method used to account for sample heterogeneity in calculating XAS (see text). The lower right panel shows how the calculated spectra are affected by nearest neighbor atoms amongst 5 of the most common O atom bonding configurations. The experimentally observed XAS is a weighted sum of each target atom configuration.

Going clockwise around the panels in Figure 11, a primitive cell taken from the Inorganic Crystal Structure Database (ICSD) was expanded and alloy atoms (either Al or Si) substituted randomly throughout the cluster. Atom positions within the cluster were then relaxed using DFT to find a low energy configuration representative of the ground state. Ten different relaxed alloys were produced for each NZP_Al and NZP_Si variant. A statistical analysis of the 6-coordinate bonding configurations for O and Na identified representative target atoms for the FEFF90 calculation (labeled O_OOOOOP, etc. in figure). It is clear from Figure 11 that each of the O_OOOOxx scattering centers produces a different XAS. By weighting the most abundant scatter configurations in the lattice, we can calculate sufficiently accurate XAS for comparison to experiment, presuming the DFT model is correct.

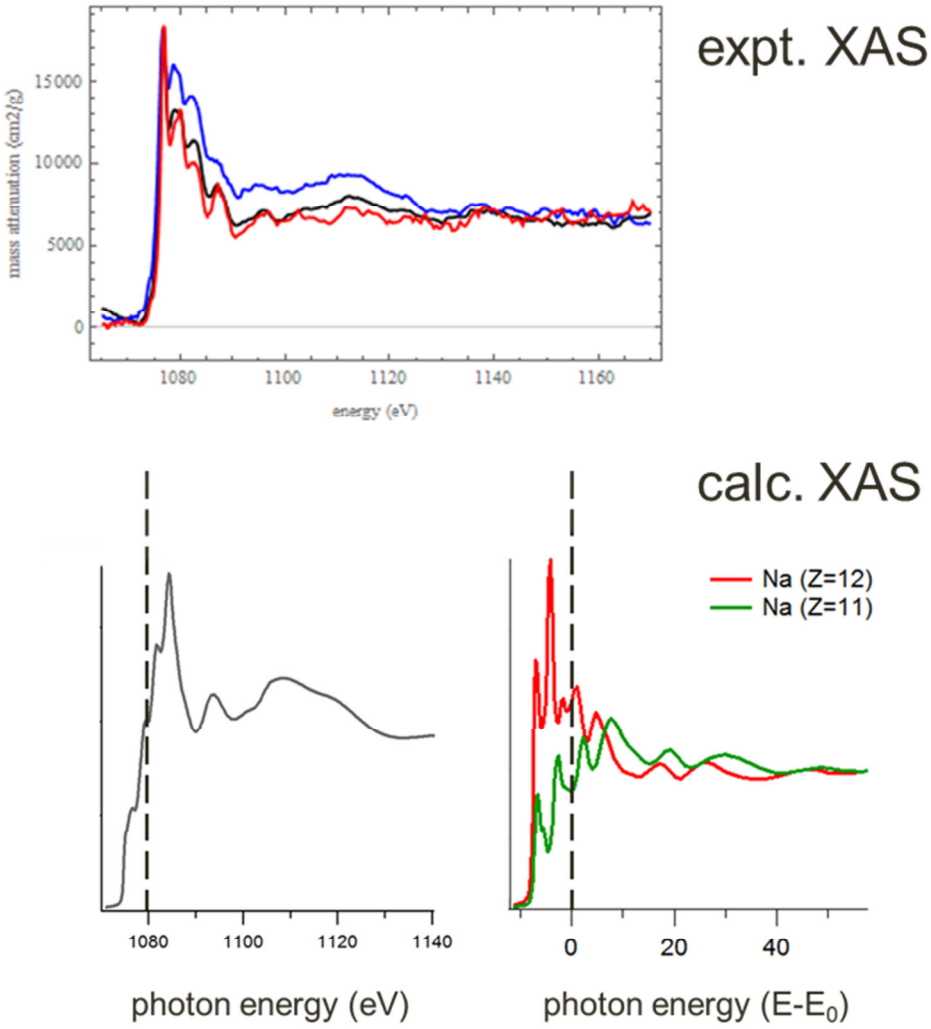

Figure 12. (top) Experimentally observed Na-K edge XAS for each of the three NaSICON compositions investigated in this LDRD. (bottom) Calculated Na-K XAS illustrating how the choice of scattering potential and final-state rule affect the calculated spectra. Here we demonstrate that a "Z+1" potential must be used to adequately model the Na 1s core hole (see text).

Additional complexity with use of FEFF90 is determining sufficient cluster size, scattering potential, and final state rules for making detailed and meaningful comparisons to experimental observations. This was particularly problematic with the Na atom, where the core hole in the final state is not adequately screened by the available Na atomic potential. This is illustrated in Figure 12 where we compare experimental XAS in the top panel to the results of FEFF90 calculations using Z=11 (Na) and Z=12 (Mg) atomic scattering potentials. Here we resorted to using the "Z+1" method described by Prado and Flank,(17) among others, to resolve the discrepancy. The results of our soft X-ray experimental campaigns and subsequent analysis are the subject of a pending technical publication.

2.4.2 Resolving Na^+ Diffusion Pathway in NZP

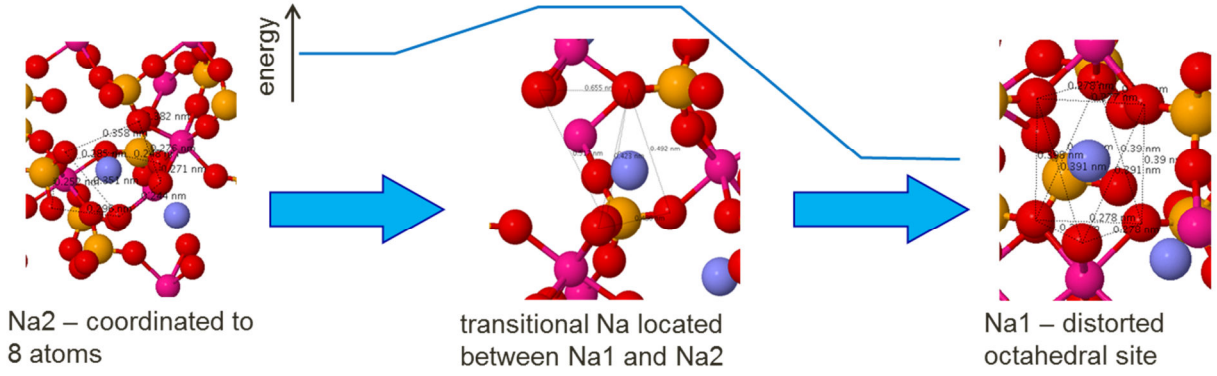

Figure 13. Schematic illustrating the diffusion pathway calculated for Na^+ in the NZP lattice, and the associated energy diagram for this process. As Na^+ transitions from the site labeled "Na2" to "Na1", it encounters a crystallographic bottleneck as shown in the center panel. DFT shows that the energy barriers to Na^+ transport are very sensitive to small lattice distortions (see text).

Using PBE exchange-correlation functionals within the VASP implementation of DFT,(13–16) we identified three important binding sites in the Na^+ conduction channel in NZP, shown in Figure 13. The "Na2" is coordinated to 8 atoms and sits in the highest energy binding site along the conduction pathway. For sodium to move through the lattice, it must pass through a "transitional" binding site, which is a crystallographically-defined bottleneck, in route to the lowest energy "Na1" site. The activation energy calculated for this process (E_a=0.5 eV) using the nudged elastic band method agrees with experiment. Furthermore, DFT revealed that the energetics for Na^+ diffusion is extremely sensitive to the lattice constant, increasing by 0.2 eV for a modest 2% decrease in the c-axis dimension. In addition, the transition state moves to the "Na2" site when the c-axis dimension is decreased. In total, these findings suggest a strategy for increasing ion conduction in NZP, and are the subject of a pending technical publication.

3. CONCLUSIONS

The objective of this LDRD project was to analyze transport chemistry in Al- and Si-substituted NaSICON materials using *in situ*, synchrotron-based X-ray diagnostics and Density Functional theory. We prepared thin-films of $NaZr_2P_3O_{12}$, $Na_{1+x}Al_xZr_{2-x}P_3O_{12}$, and $Na_{1+x}Zr_2Si_xP_{3-x}O_{12}$ NaSICONs via chemical solution deposition on platinized silicon and aluminum nitride substrates. Depending on the film stoichiometry and annealing temperature, various film textures, ion conductivities, and phase impurities were obtained. While Na^+ ion conductivity, measured using impedance spectroscopy, showed that addition of Al and Si resulted in films with much higher conductance than the baseline NZP ($NaZr_2P_3O_{12}$) material, general trends in the Si variant were also observed; 1) increasing silicon content from x=0.25 to x=1.0 resulted in a decrease in crystallographic texture and average crystallite size, 2) increasing process temperature increased the average crystallite size for each composition, 3) the highest room-temperature ionic conductivity was observed for the x=0.25 composition processed at 800 °C, and 4) the observed trends of decreasing ionic conductivity with increasing silicon content can be attributed to a decrease in crystallite size.

A key differentiating element to the approach taken in this LDRD was assessing the effects of the bonding environment local to the Na and O atoms on mobility using synchrotron X-ray spectroscopies. To accomplish this we deployed an experimental platform suitable for X-ray Raman measurements at SSRL and a Sandia-designed, robust fluorescence yield detector at ALS. Five experimental campaigns where conducted at two synchrotrons over the course of this project. We tested the feasibility of using hard X-ray Raman spectroscopy to overcome spectral interference from molecular O_2 and H_2O, we collected *in situ* soft X-ray K-edge XAS on O and Na atoms for $NaZr_2P_3O_{12}$, $Na_{1.25}Al_{0.25}Zr_{1.75}P_3O_{12}$, and $Na_{1.5}Zr_2Si_{0.5}P_{2.5}O_{12}$ thin films under partial pressures of O_2 and H_2O at elevated temperature, tested the efficacy of using TEM HREELS to supplement the information provided by X-ray XAS, and ultimately discovered that Al and Si substitution into our base NaSICON formulation ($NaZr_2P_3O_{12}$) has a significant effect on the local bonding environment for Na and O atoms in the lattice.

Finally, we applied Density Functional Theory to interpret the experimental observations and provide a critical link to atomistic processes that underpin and influence ion transport. Electronic structure models for $NaZr_2P_3O_{12}$, $Na_{1.25}Al_{0.25}Zr_{1.75}P_3O_{12}$, and $Na_{1.5}Zr_2Si_{0.5}P_{2.5}O_{12}$ were derived from alloying and relaxing known structures. We formulated a methodology for applying a parameter-free, *ab initio* physics code for predicting XAS in heterogeneous systems and are in the process of validating the DFT structure models against the XAS observations. In the interim, we did find agreement between DFT and experiment for Na^+ conduction energetics (*i.e.*, activation energies measured by impedance spectroscopy), and that the diffusion barrier is very sensitive to lattice constant and ion channel size. For example, a few tenths of an angstrom difference in lattice spacing causes tenths of an eV change in the diffusion barrier. Given this, we now have the ability to theoretically formulate appropriately chosen substitutional defects that could considerably increase ion conductivity in NaSICON.

4. REFERENCES

1. N. Anantharamulu, K. Koteswara Rao, G. Rambabu, B. Vijaya Kumar, V. Radha, and M. Vithal, *J. Mater. Sci.*, **46**, 2821–2837 (2011).

2. P. P. Kumar and S. Yashonath, *J. Phys. Chem. B*, **106**, 7081–7089 (2002).

3. J. J. Rehr, J. J. Kas, F. D. Vila, M. P. Prange, and K. Jorissen, *Phys. Chem. Chem. Phys.*, **12**, 5503 (2010).

4. N. Gasmi, N. Gharbi, H. Zarrouk, P. Barboux, R. Morineau, and J. Livage, *J. Sol-Gel Sci. Technol.*, **4**, 231–237 (1995).

5. A. Martucci, S. Sartori, M. Guglielmi, M. L. Di Vona, S. Licoccia, and E. Traversa, *J. Eur. Ceram. Soc.*, **22**, 1995–2000 (2002).

6. W. Meier, C. Apblett, D. Ingersoll, A. McDaniel, and J. F. Ihlefeld, *J. Electrochem. Soc.*, **161**, A364–A367 (2014).

7. F. de Groot, M. Grioni, J. Fuggle, J. Ghijsen, G. Sawatzky, and H. Petersen, *Phys. Rev. B*, **40**, 5715–5723 (1989).

8. D. Sokaras, D. Nordlund, T.-C. Weng, R. A. Mori, P. Velikov, D. Wenger, A. Garachtchenko, M. George, V. Borzenets, and B. Johnson, *Rev. Sci. Instrum.*, **83**, 043112–043112 (2012).

9. K. F. McCarty, M. Monti, S. Nie, D. A. Siegel, E. Starodub, F. El Gabaly, A. H. McDaniel, A. Shavorskiy, T. Tyliszczak, H. Bluhm, et al., *J. Phys. Chem. C*, **118**, 19768–19777 (2014).

10. A. H. McDaniel, W. C. Chueh, A. Shavorskiy, T. Tyliszczak, H. Bluhm, K. F. McCarty, and F. El Gabaly, *ECS Trans.*, **58**, 47–53 (2013).

11. A. Manceau, M. A. Marcus, and S. Grangeon, *Am. Mineral.*, **97**, 816–827 (2012).

12. C. T. Chantler, *J. Phys. Chem. Ref. Data*, **24**, 71 (1995).

13. G. Kresse and J. Hafner, *Phys. Rev. B*, **47**, 558–561 (1993).

14. G. Kresse and J. Hafner, *Phys. Rev. B*, **49**, 14251–14269 (1994).

15. G. Kresse and J. Furthmüller, *Comput. Mater. Sci.*, **6**, 15–50 (1996).

16. G. Kresse and J. Furthmüller, *Phys. Rev. B*, **54**, 11169–11186 (1996).

17. R. J. Prado and A. M. Flank, *Phys. Scr.*, **2005**, 165 (2005).

DISTRIBUTION

1	MS0613	David Ingersoll	02500
1	MS1411	Paul Clem	01816
1	MS9161	Sarah Allendorf	08340
1	MS9161	Jonathan Zimmerman	08367
1	MS0899	Technical Library	09536 (electronic copy)
1	MS0359	D. Chavez, LDRD Office	01911


Sandia National Laboratories